Structure and properties of 2-cyanopyridinium perchlorate [2-CNPyH][ClO_4]

2006 J. Phys.: Condens. Matter 18 3307

(http://iopscience.iop.org/0953-8984/18/12/012)

INSTITUTE OF PHYSICS PUBLISHING JOURNAL OF PHYSICS: CONDENSED MATTER

J. Phys.: Condens. Matter **18** (2006) 3307–3324 doi:10.1088/0953-8984/18/12/012

Structure and properties of 2-cyanopyridinium perchlorate [2-CNPyH][ClO_4]

O Czupiński[1], M Wojtaś[1], J Zaleski[2], R Jakubas[1] and W Medycki[3]

[1] Faculty of Chemistry, University of Wrocław, Joliot–Curie 14, 50-383 Wrocław, Poland
[2] Institute of Chemistry, University of Opole, Oleska 48, 45-951 Opole, Poland
[3] Institute of Molecular Physics, Polish Academy of Science, Smoluchowskiego 17, 60-179 Poznań, Poland

E-mail: maciekwo@wcheto.chem.uni.wroc.pl

Received 14 July 2005, in final form 16 February 2006
Published 9 March 2006
Online at stacks.iop.org/JPhysCM/18/3307

Abstract

The crystal structure of 2-cyanopyridinium perchlorate, [2-CNPyH][ClO_4], has been determined at 100 (phase II) and 293 K (phase I). It is monoclinic $P2_1$ at 100 K and orthorhombic $P2_12_12_1$ at 293 K. The dynamic properties of the crystal were studied by differential scanning calorimetry, dilatometry, pyroelectric, dielectric, proton (^{1}H NMR), chlorine (^{35}Cl NMR) magnetic resonance spectroscopies and the infrared method. The crystal undergoes a structural phase transition (I → II) at 170 K characterized by a complex mechanism involving both 'order–disorder' and 'displacive' contributions. It reveals pyroelectric properties below 170 K. The dielectric relaxation existing over phase I is due to the motion of the cyano group, whereas the dynamics of the $[ClO_4]^-$ anions is reflected in the significant dielectric increment around the I → II phase transition.

1. Introduction

Recently, much attention has been devoted to simple hybrid organic/inorganic systems due to their interesting nonlinear physical properties. The heteroaromatic pyridine cations with BF_4^-, ClO_4^-, ReO_4^-, IO_4^-, FSO_3^- and $FCrO_3^-$ anions form a large group of molecular–ionic crystals showing ferroelectric properties [1–3]. Lately, a new analogue containing the pentagonal aromatic ring such as imidazolium cations, $[C_3N_2H_5][BF_4]$, appeared also to have ferroelectric ordering [4]. In all prototypes of these crystals the aromatic cations are highly disordered, revealing rapid reorientation within the aromatic ring. Slowing down this motion and partial ordering of the dipolar moieties in the respective mesophases lead to the appearance of ferroelectricity.

In the search for polar materials we extended our studies to simple ionic salts with substituted pyridinium cation such as 4-aminopyridinium: [4-NH_2PyH][ClO_4] [5] and

[4-NH_2PyH][BF_4] [6]. It should be emphasized that heteroaromatic cations are bestowed with a permanent dipole moment. The interactions of cations with the monovalent tetrahedral counter anions (e.g. ClO_4^-, BF_4^-) are expected to generate interesting dielectric properties of crystals. Both analogues reveal structural phase transitions attributed to the dynamics of the organic cations. [4-NH_2PyH][ClO_4] disclosed ferroic (ferroelastic) and pyroelectric properties below 241 K. The second derivative, [4-NH_2PyH][BF_4], is characterized by a rich sequence of phase transitions (at 250, 281, 388 and 485 K) and ferroic (ferroelastic) properties in the low-temperature phases. It was shown that all the phase transitions are due to the change in the dynamical state of the 4-aminopyridinium and tetraborate or perchlorate moieties.

Recently we have synthesized a molecular–ionic compound with the crystal structure comprising the 2-cyanopyridinium cation, [2-CNPyH][ClO_4]. In this paper we report x-ray, calorimetric, dielectric, pyroelectric and magnetic resonance (^{1}H and ^{35}Cl NMR) studies of this crystal over a wide temperature range. Vibrational (infrared) studies as a function of temperature are also presented. A possible mechanism of the structural phase transition in [2-CNPyH][ClO_4] is proposed.

2. Experimental details

2-cyanopyridinium perchlorate was prepared by the stoichiometric reaction of 2-cyanopyridine with perchloric acid. The obtained salt was recrystallized twice from aqueous solution. The single crystals of [2-CNPyH][ClO_4] were grown by slow evaporation at 300 K.

Measurements were performed with an Oxford Diffraction KM4 CCD κ-axis diffractometer with graphite monochromated Mo Kα ($\lambda = 0.710\,73$ Å) radiation. Two data sets were collected: one at 293(2) K, the other one at 100.0(1) K. The low temperature was stabilized using an Oxford Cryosystem open flow cooler. The temperature stability was of the order of ± 0.1 K. At 293 K a total of 6812 reflections with 2241 independent ($R_{\mathrm{int}} = 0.028$) were measured in the 2Θ range $6^\circ \leqslant 2\Theta \leqslant 59^\circ$ using the ω–Θ scan technique, whereas at 100 K a total of 6834 were measured with 3576 independent ($R_{\mathrm{int}} = 0.1019$). Lorentz and polarization corrections were applied. The structures were solved by the direct method and refined by a full-matrix least-squares method. All hydrogen atoms were included from the difference Fourier synthesis. The SHELX-97 [7, 8] program was used for the structure solution and refinement. The structure drawings were prepared using SHELXTL program [9]. The details of the data collection and processing are listed in table 1. Crystallographic data for the structures reported in this paper (excluding structure factors) have been deposited with the Cambridge Crystallographic Data Centre, CCDC no. 270367 (100 K) and CCDC 270368 (293 K). Copies of this information may be obtained free of charge from the CCDC, 12 Union Road, Cambridge CB2 1EZ, UK (fax: +44-1223-336033; e-mail: deposit@ccdc.cam.ac.uk or http://www.ccdc.cam.ac.uk).

The complex electric permittivity, $\epsilon^* = \epsilon' - \mathrm{i}\epsilon''$, was measured with an HP 4284A Precision LCR Meter in the frequency range between 75 Hz and 1 MHz and in the 80–300 K range. The dimensions of the sample were of the order of $5 \times 5 \times 1$ mm^3. The overall error for the real and imaginary parts of the complex electric permittivity was less than 5% and 10%, respectively. The spontaneous polarization was measured between 100 and 240 K by a charge integration technique using a Keithley 617 Programmable Electrometer. The temperature was stabilized by an Instec STC 200 temperature controller. Differential scanning calorimetry (DSC) measurements were carried out using a Perkin Elmer DSC-7 in the temperature range 100–450 K. Thermogravimetric analysis (TGA) and differential thermal analysis (DTA) were made on a Setaram SETSYS 16/18 instrument in nitrogen atmosphere, with sample mass 14.94 mg and heating rate 2 K min^{-1}, in the temperature range

Table 1. Crystal data and structure refinement for [2-CNPyH][ClO_4] at 100 and 293 K.

Empirical formula	$C_6\,H_5\,Cl\,N_2\,O_4$	
Formula weight	204.57	
Temperature	100.0(1) K	293(2) K
Wavelength	0.710 73 Å	
Crystal system, space group	Monoclinic, $P2_1$	Orthorhombic, $P2_12_12_1$
Unit cell dimensions	$a = 9.802(2)$ Å	$a = 7.585(1)$ Å
	$b = 7.617(2)$ Å	$b = 10.079(1)$ Å
	$c = 11.314(3)$ Å	$c = 11.434(1)$ Å
	$\beta = 90.11(2)^\circ$	
Volume	844.7(3) Å^3	874.09(11) Å^3
Z, calculated density	4, 1.609 Mg m^{-3}	4, 1.555 Mg m^{-3}
Absorption coefficient	0.435 mm^{-1}	0.421 mm^{-1}
F(000)	416	
Crystal size	0.3 × 0.3 × 0.2 mm^3	
Θ range for data collection	3.84°–29.51°	3.22°–29.55°
Index ranges	$-13 \leqslant h \leqslant 12$,	$-10 \leqslant h \leqslant 5$,
	$-10 \leqslant k \leqslant 9$,	$-13 \leqslant k \leqslant 13$,
	$-15 \leqslant l \leqslant 15$	$-15 \leqslant l \leqslant 15$
Reflections collected/unique	6834/3576 ($R_{(int)} = 0.086$)	6812/2241 ($R_{(int)} = 0.0283$)
Refinement method	Full-matrix least-squares on F^2	
Data/restraints/parameters	3576/1/235	2241/0/120
Goodness-of-fit on F^2	0.982	1.103
Final R indices [$I > 2\sigma(I)$]	$R_1 = 0.0567$, w$R_2 = 0.1401$	$R_1 = 0.0310$, w$R_2 = 0.0833$
R indices (all data)	$R_1 = 0.0656$, w$R_2 = 0.1480$	$R_1 = 0.0339$, w$R_2 = 0.0918$
Absolute structure parameter	−0.07(9)	0.53(6)
Largest diff. peak and hole	0.567 and $-0.751e$ Å^{-3}	0.182 and $-0.270e$ Å^{-3}

300–700 K. The dilatometric measurements were carried out with a Perkin Elmer TMA-7 thermomechanical analyser between 100 and 500 K. The dimensions of the sample were of the order of $8\times5\times1.5$ mm^3. The proton spin–lattice relaxation time T_1 was measured with a Bruker SXP 4-100 spectrometer working at the frequency of 90 MHz. The temperature of the sample was automatically stabilized by the standard Bruker liquid nitrogen system. The T_1 relaxation times were determined by the saturation method. The powdered samples of [2-CNPyH][ClO_4] were degassed under pressure of 10^{-5} Torr and sealed under vacuum in glass ampoules. The ^{35}Cl NMR measurements were performed at a magnetic field of $B_0 = 7.05$ T corresponding to a resonance frequency of 29.44 MHz, using an MSL 300 NMR Bruker spectrometer. ^{35}Cl NMR measurements were made on powdered samples. The substance was filled into glass tubes with a diameter of 5 mm. Only the central transitions were measured. The infrared spectra (4000–400 cm^{-1}) were measured by using a Nicolet Nexus spectrometer with a resolution 1.0 cm^{-1}. The spectra were recorded in Nujol mulls and KBr windows. For the FT-FIR region (500–50 cm^{-1}) a Bruker IFS66 spectrometer was used to record the spectra of the powder samples in Nujol with polyethylene discs at room temperature. A variable-temperature cell (Graseby–Specac) was used for measurements of the spectra as a function of temperature in the 90–290 K range. The stability of the temperature was ± 1 K.

3. Results and discussion

3.1. Crystal structure of [2-*CNPyH*][*ClO*$_4$]

At room temperature the structure was solved in the orthorhombic space group $P2_12_12_1$. On lowering the temperature below the phase transition some of the diffraction peaks are split. This

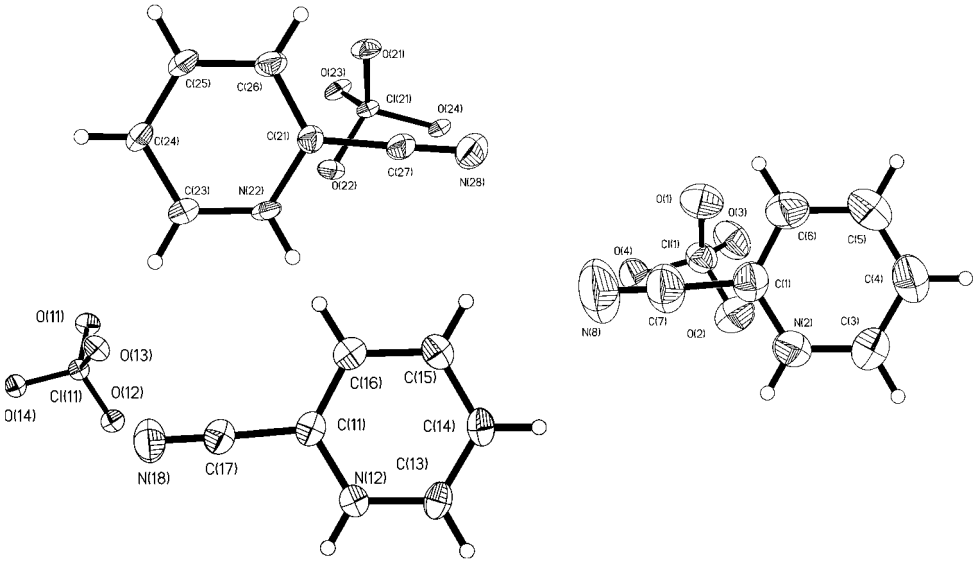

Figure 1. Atom numbering scheme of the [2-CNPyH][ClO_4] crystal at 100 K (the left-hand side) and at 293 K (the right-hand side).

indicates lowering of the symmetry and change of the crystal system at T_c. In performing data reduction it is impossible to eliminate one set of split reflections, since some of them overlap. To solve the structure and get the best results we lowered the temperature to the lowest attainable (100 K). On data reduction we assumed initially a triclinic system. In the Xprep program we obtained the same $R_{int} = 0.15$ for the initial orthorhombic $P2_12_12_1$ group and two monoclinic $P2_1$ space groups. For the third $P2_1$ group the R_{int} was the lowest ($R_{int} = 0.086$). The lowest final R was also obtained for the solution in this monoclinic space group (see table 1). The ferroic phase transition may be described as 222F2. The number of independent parameters is increased from 120 at 293 K to 235 at 100 K. In the independent part of the unit cell there are one cation and one anion at room temperature and twice as many below the phase transition. Figure 1 presents the atom numbering at both temperatures. Figure 2 shows the perspective view of the [2-CNPyH][ClO_4] crystal at two temperatures. Selected bond lengths and angles for the crystal at 100 and 293 K are listed in table 2.

The phase transition is believed to be most probably of a 'displacive' type. It results in the change of the hydrogen bonding scheme (see table 3). The changes in the geometry and strength of the N–H $\cdots$ O hydrogen bonds are found to be rather small. The lowering of temperature leads to the decrease of the N $\cdots$ O distance of the order of 0.025(4) Å. The significant changes on lowering temperature in the geometry of hydrogen bonds are observed in the C–H $\cdots$ O bonds. The relevant C $\cdots$ O distances at both temperatures are in one case significantly different. In the case of the C(6)–H(6) $\cdots$ O(3) bond at 293 K, which is described below the phase transition as a pair of bonds (C(16)–H(16) $\cdots$ O(23) and C(26)–H(26) $\cdots$ O(13)), the geometry of that bond does not change (table 3). The decrease of the C $\cdots$ O distance on lowering the temperature is the same as that for the N $\cdots$ O distance (0.025(6) Å).

Large changes are seen, however, in the C(4)–H(4) $\cdots$ O(1) hydrogen bond. At 293 K the C(4) $\cdots$ O(1) distance is 3.375(3) Å, whereas below the phase transition C(14) $\cdots$ O(23) and C(24) $\cdots$ O(13) bond lengths are 3.239(6) Å and 3.224(6) Å, respectively. The changes are 0.136(6) Å and 0.151(6) Å, respectively. It should be noted that below the phase transition

Table 2. Selected bond lengths and angles for [2-CNPyH][ClO_4] at 100 and 293 K.

293 K			
Cl(1)–O(3)	1.424(2)	O(1)–Cl(1)–O(2)	110.6(1)
Cl(1)–O(1)	1.427(2)	O(3)–Cl(1)–O(4)	108.5(1)
Cl(1)–O(2)	1.430(2)	O(1)–Cl(1)–O(4)	109.8(1)
Cl(1)–O(4)	1.453(2)	O(2)–Cl(1)–O(4)	108.6(1)
C(1)–N(2)	1.338(2)	N(2)–C(1)–C(6)	120.8(2)
C(1)–C(6)	1.361(3)	N(2)–C(1)–C(7)	117.2(2)
C(1)–C(7)	1.443(3)	C(6)–C(1)–C(7)	122.0(2)
N(2)–C(3)	1.326(2)	C(3)–N(2)–C(1)	121.6(2)
C(3)–C(4)	1.370(3)	N(2)–C(3)–C(4)	120.0(2)
C(4)–C(5)	1.362(3)	C(5)–C(4)–C(3)	119.4(2)
C(5)–C(6)	1.389(3)	C(4)–C(5)–C(6)	120.1(2)
C(7)–N(8)	1.120(3)	C(1)–C(6)–C(5)	118.0(2)
O(3)–Cl(1)–O(1)	109.6(1)	N(8)–C(7)–C(1)	177.3(4)
100 K			
Cl(21)–O(23)	1.433(3)	O(23)–Cl(21)–O(24)	109.2(2)
Cl(21)–O(21)	1.442(2)	O(21)–Cl(21)–O(24)	109.1(2)
Cl(21)–O(22)	1.442(3)	O(22)–Cl(21)–O(24)	108.6(2)
Cl(21)–O(24)	1.458(3)	O(13)–Cl(11)–O(11)	109.5(2)
Cl(11)–O(13)	1.434(3)	O(13)–Cl(11)–O(12)	110.2(2)
Cl(11)–O(11)	1.442(2)	O(11)–Cl(11)–O(12)	110.3(2)
Cl(11)–O(12)	1.444(3)	O(13)–Cl(11)–O(14)	109.2(2)
Cl(11)–O(14)	1.461(3)	O(11)–Cl(11)–O(14)	109.3(2)
C(11)–N(12)	1.346(6)	O(12)–Cl(11)–O(14)	108.3(2)
C(11)–C(16)	1.359(6)	N(12)–C(11)–C(16)	121.4(4)
C(11)–C(17)	1.466(6)	N(12)–C(11)–C(17)	116.0(4)
N(12)–C(13)	1.342(6)	C(16)–C(11)–C(17)	122.6(4)
C(13)–C(14)	1.362(7)	C(13)–N(12)–C(11)	120.8(4)
C(14)–C(15)	1.389(7)	N(12)–C(13)–C(14)	120.6(4)
C(15)–C(16)	1.401(6)	C(13)–C(14)–C(15)	119.6(4)
C(17)–N(18)	1.120(6)	C(14)–C(15)–C(16)	119.0(4)
C(21)–N(22)	1.348(5)	C(11)–C(16)–C(15)	118.6(4)
C(21)–C(26)	1.366(5)	N(18)–C(17)–C(11)	177.9(5)
C(21)–C(27)	1.450(6)	N(22)–C(21)–C(26)	120.3(4)
N(22)–C(23)	1.324(6)	N(22)–C(21)–C(27)	117.0(3)
C(23)–C(24)	1.388(6)	C(26)–C(21)–C(27)	122.7(4)
C(24)–C(25)	1.374(6)	C(23)–N(22)–C(21)	122.1(3)
C(25)–C(26)	1.397(6)	N(22)–C(23)–C(24)	120.3(4)
N(28)–C(27)	1.131(6)	C(25)–C(24)–C(23)	118.6(4)
O(23)–Cl(21)–O(21)	109.6(2)	C(24)–C(25)–C(26)	120.2(4)
O(23)–Cl(21)–O(22)	110.0(2)	C(21)–C(26)–C(25)	118.5(4)
O(21)–Cl(21)–O(22)	110.4(2)	N(28)–C(27)–C(21)	178.6(5)

two new sets of hydrogen bonds additionally appear (table 3). They are relatively weak and are probably connected with the freezing of librations of the molecule.

Hydrogen bond net and coulombic forces are responsible for interactions between moieties in the [2-CNPyH][ClO_4] crystal. The 2-cyanopyridinium cations are organized in the polymer-like structure along the *c*-axis, where the neighbouring cations are connected to each other through $[ClO_4]^-$ anions via hydrogen bonds in the following sequence: C(6)–H(6) $\cdots$ O(3)–Cl(1)–O(4) $\cdots$ H(2)′–N(2)′, etc. The neighbouring cations are twisted

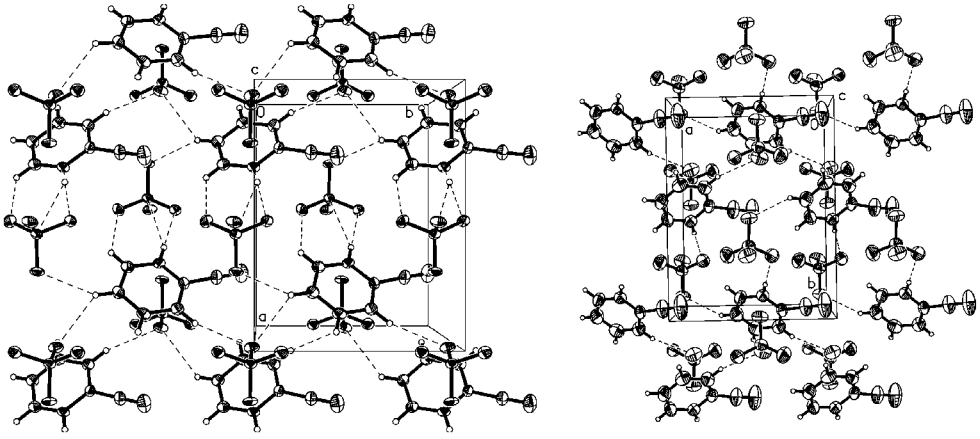

Figure 2. Perspective view of the [2-CNPyH][ClO_4] crystal at 100 K (the left-hand side) and at 293 K (the right-hand side).

Table 3. Selected hydrogen bond lengths and angles for [2-CNPyH][ClO_4] at 100 and 293 K.

D–H $\cdots$ A	d(D–H)	d(H $\cdots$ A)	d(D $\cdots$ A)	<(DHA)
		293 K		
N(2)–H(2) $\cdots$ O(4)[a]	0.86	1.97	2.829(2)	173
C(4)–H(4) $\cdots$ O(1)[b]	0.93	2.53	3.375(3)	151
C(6)–H(6) $\cdots$ O(3)[c]	0.93	2.44	3.345(3)	164
Symmetry transformations used to generate equivalent atoms: [a] $-1/2+x, 1/2-y, 1-z$. [b] $-1+x, y, z$. [c] $1-x, -1/2+y, 1/2-z$				
		100 K		
N(12)–H(12) $\cdots$ O(14)[d]	0.86	1.95	2.803(4)	172
C(13)–H(13) $\cdots$ O(12)[d]	0.93	2.57	3.220(5)	127
C(14)–H(14) $\cdots$ O(11)[f]	0.93	2.5	3.353(6)	153
C(14)–H(14) $\cdots$ O(23)[g]	0.93	2.56	3.239(6)	130
C(16)–H(16) $\cdots$ O(23)[h]	0.93	2.42	3.321(6)	162
N(22)–H(22) $\cdots$ O(24)[e]	0.86	1.95	2.806(4)	173
C(23)–H(23) $\cdots$ O(22)[e]	0.93	2.55	3.208(5)	128
C(24)–H(24) $\cdots$ O(21)[i]	0.93	2.49	3.344(6)	152
C(24)–H(24) $\cdots$ O(13)[i]	0.93	2.55	3.224(6)	130
C(26)–H(26) $\cdots$ O(13)	0.93	2.42	3.320(6)	162
Symmetry transformations used to generate equivalent atoms: [d] $-x, 1/2+y, 1-z$. [e] $1-x, -1/2+y, 1-z$. [f] $1+x, 1+y, 1+z$. [g] $x, 1+y, 1+z$ [h] $-x, 1/2+y, 1-z$. [i] $x, -1+y, z$				

with respect to each other by an angle of 81.6(6)°. It should be emphasized that the cyano nitrogen atom does not interact via hydrogen bonds with other atoms in both phases. This causes the cyano group to possess in phase I (the high-temperature one) quite a large reorientational freedom and it results in an enlargement of thermal ellipsoids of related atoms. The value of one third of the trace of the orthogonalized U_{ij} tensor, U_{eq}, of the cyano N atom is twice as big as the U_{eq} of other atoms. A similar situation is observed in the low-temperature phase, but the difference is smaller (U_{eq} (cyano N)/U_{eq} (mean of other atoms) is 106/57 and

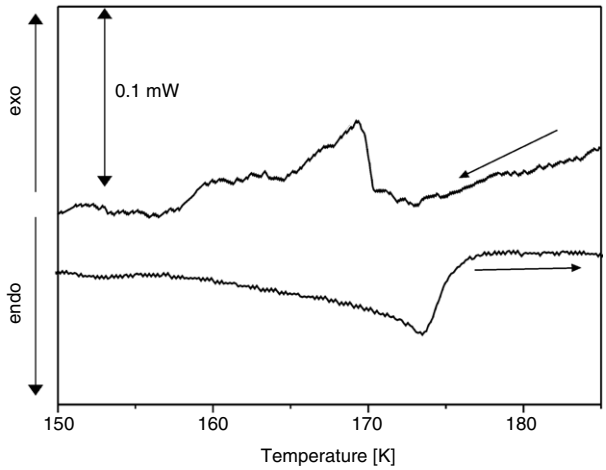

Figure 3. DSC curves of the [2-CNPyH][ClO_4] crystals for the cooling and heating runs (10 K min^{-1}).

42/25 at 293 and 100 K, respectively). The pyridinium ring of 2-cyanopyridine seems to be perfectly planar—the mean deviation from the plane equals zero within error limits at 293 and at 100 K. The cyano group deviates from the pyridinium ring by an angle of 33.5(4)°. The interatomic distances and angles of 2-cyanopyridine, as well as slightly distorted tetrahedrons of $[ClO_4]^-$, are in agreement with those found elsewhere [10–14].

3.2. Thermal behaviour

Figure 3 presents the results of the calorimetric measurements of the powdered sample of [2-CNPyH][ClO_4]. The well reversible thermal anomaly at 170 K is related to the phase transition. DSC measurements were carried out with different scan rates (5, 10 and 20° min^{-1}). The phase transition temperature was determined by the extrapolation of the scan rate to 0° min^{-1} and then the temperature hysteresis was not observed. The shape of the anomaly and the lack of the temperature hysteresis indicate that the phase transition is of the continuous type.

The dilatometric curves in the vicinity of the phase transition are presented in figure 4. The measurements were performed along the following crystallographic directions (according to the high-temperature orthorhombic symmetry): a, $[01\bar{1}]$, c. The measurements were not carried out along the b-axis, because we did not succeed in preparing the sample with this orientation (only the a and c directions were reflected in the morphology of the single crystal). The dilatometric anomaly at about 170 K is characteristic for a continuous phase transition, which is in agreement with the calorimetric studies. The phase transition is manifested only by the change in the linear thermal expansion coefficient's value ($\alpha = \frac{d(\Delta L/L_0)}{dT}$) along the a as well as c direction, whereas no anomaly was observed along the $[01\bar{1}]$ direction at T_c. It is worth noting that α_c changes its sign from positive in the orthorhombic phase to negative in the monoclinic phase.

In order to determine the thermal stability of [2-CNPyH][ClO_4], simultaneous thermogravimetric analysis (TGA) and differential thermal analysis (DTA) was carried out. The results are shown in figure 5. The first peak at 387 K is related to a simultaneous melting and partial decomposition of the sample. The sample mass is decreased by about 30%. Two next peaks at 477 and 540 K are related to further mass loss up to 90% at 700 K.

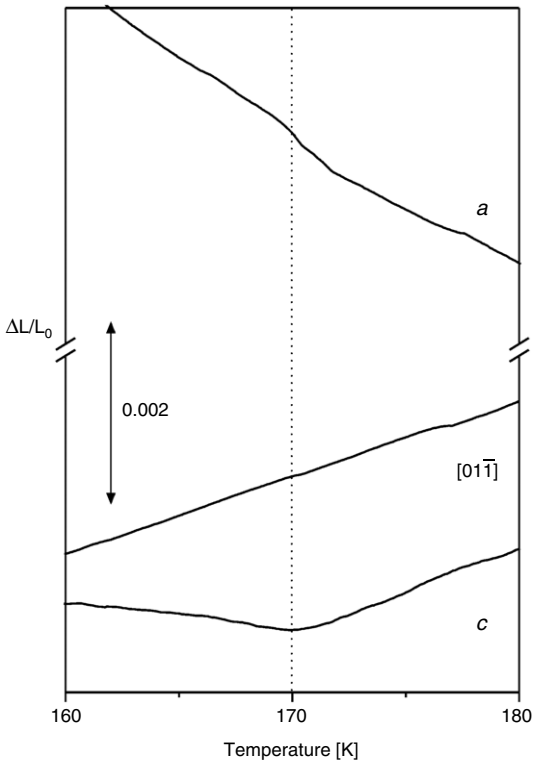

Figure 4. The linear thermal expansion of the [2-CNPyH][ClO_4] crystal (3 K min^{-1}).

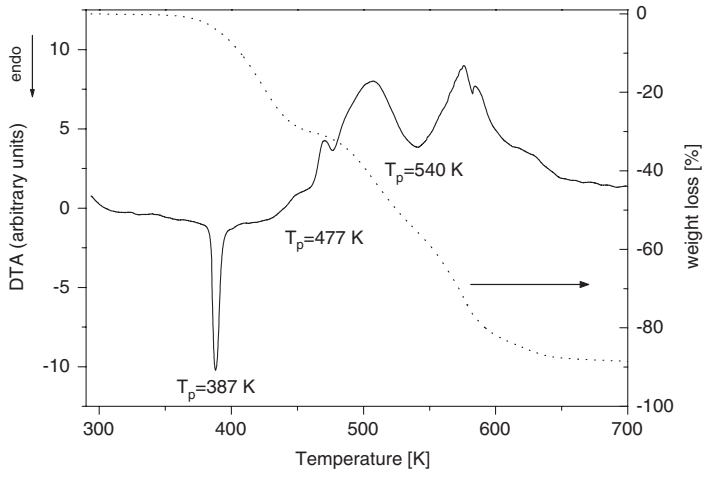

Figure 5. Simultaneous curves of thermogravimetric analysis and differential thermal analysis (2 K min^{-1}).

3.3. Pyroelectric measurements

The x-ray studies showed that the phase transition at 170 K is connected with the presence of the polar diad axis ($P2_1$). The measurements of the pyroelectric current were carried out, to confirm the result of structural studies as well as to study the polar properties of the [2-CNPyH][ClO_4] crystal. The measurements were performed along the *a*-axis of the orthorhombic phase, which corresponds to the polar *b*-axis in the monoclinic phase (see table 1).

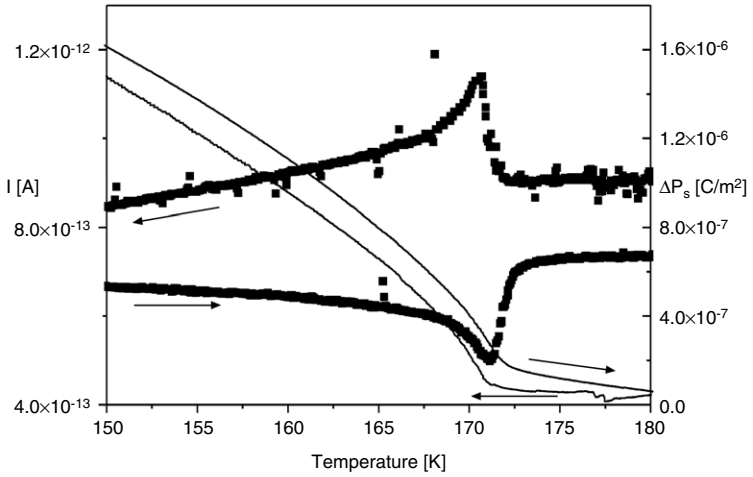

Figure 6. The temperature dependence of the pyroelectric current, I, and the spontaneous polarization change, ΔP_s, measured along the a-axis (phase I) of the [2-CNPyH][ClO_4] crystal.

The results of pyroelectric current measurements are presented in figure 6. The phase transition is manifested as a peak of the pyroelectric current. Since the pyroelectric method does not allow us to determine the absolute value of P_s for the phases I and II, only the changes in the spontaneous polarization, ΔP_s, at T_c were detected. The saturated value of ΔP_s was found to be of the order of 1.6×10^{-6} C m^{-2} at 150 K. The polarization current peaks are perfectly reversible on cooling and heating; their shape as well as the shape of the spontaneous polarization curves and the lack of the temperature hysteresis confirm the character of the phase transition as clearly continuous type. In order to check whether the studied crystal may possess ferroelectric properties attempts at the reversal of P_s by means of an external dc electric field were carried out. Unfortunately, the polarization did not reverse under a dc field intensity up to 300 kV m^{-1}. This means that below 170 K the title crystals exhibits pyroelectric properties. It should also be added that the relatively small value of P_s, being of the order of 10^{-6} C m^{-2}, is characteristic for pyroelectric materials. It should be stressed that the [2-CNPyH][ClO_4] crystal, in the low-temperature phase, is a polar material, which is in agreement with our x-ray studies.

3.4. Dielectric studies

Figure 7 presents the results of the dielectric measurements carried out along three directions: [100], [01$\bar{1}$] and [001]. The characteristic feature of the studied crystal is a clear anisotropy of the dielectric properties. The real part of the electric permittivity along the a direction, ϵ'_a, versus temperature remains constant over the high-temperature phase, with the ϵ'_a value being equal to 15, and continuously decreasing in the low-temperature (monoclinic) phase on cooling. Such a behaviour of the [2-CNPyH][ClO_4] crystals in the monoclinic phase is common for all studied directions. The strongest manifestation of the anisotropy is observed in the orthorhombic phase by the shape and values of the electric permittivity. The highest value of the electric permittivity is observed in the c direction. The value of ϵ'_c is equal to about 18 units at the room temperature. It increases to 24 units at T_c and then falls to about 6 units at 90 K. It is worth noting that the c-axis is nearly parallel to the direction of extension of the polymer-like 2-cyanopyridinium-perchlorate units (see section 3.1). The electric permittivity, $\epsilon'_{[01\bar{1}]}$, decreases

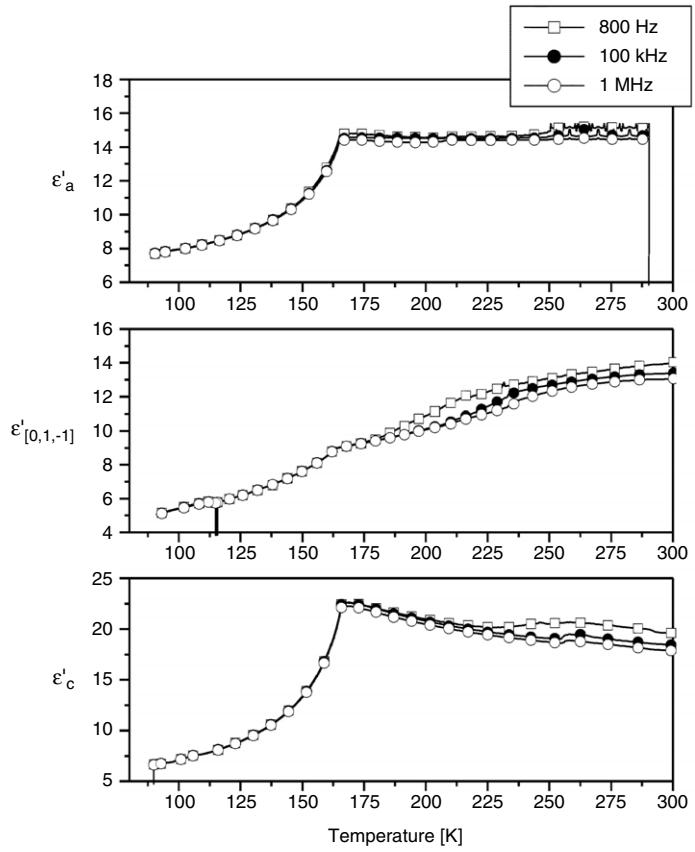

Figure 7. The temperature dependence of the real part of the complex electric permittivity measured along the a (ϵ'_a), $[0,1,\bar{1}]$ ($\epsilon'_{[0,1,\bar{1}]}$) and c (ϵ'_c) axes (on cooling).

over both the high-temperature and the low-temperature phases with decreasing temperature. The feature which significantly distinguishes this direction from the other ones is a relaxation process observed above 170 K. The dielectric dispersion is visible above the phase transition temperature in the studied frequency range (800 Hz–1 MHz). In figure 8 the real, ϵ', and imaginary, ϵ'', parts of the complex electric permittivity are presented (the left-hand side) as well as the Cole–Cole diagrams at selected temperatures and the Arrhenius plot (the right-hand side).

The relaxation process was analysed in order to estimate the dielectric activation parameters. The dielectric response in the [2-CNPyH][ClO_4] salt is well described by the Cole–Cole relation:

$$\epsilon^* = \epsilon_\infty + \frac{\epsilon_0 - \epsilon_\infty}{1 + (\mathrm{i}\omega\tau)^{1-\alpha}} \tag{1}$$

where ϵ_0 and ϵ_∞ are the low- and high-frequency limits of the electric permittivity, respectively, ω is the angular frequency, τ is the macroscopic relaxation time and α is the distribution of the relaxation times parameter. We have fitted the experimental Argand plots at several temperatures with equation (1) and determined the fitting parameters ϵ_0, ϵ_∞, τ and α. Since the strength of the dielectric relaxator is small, one can assume that we are dealing with a non-interacting dipole system, thus the macroscopic relaxation time, τ, is treated as a microscopic

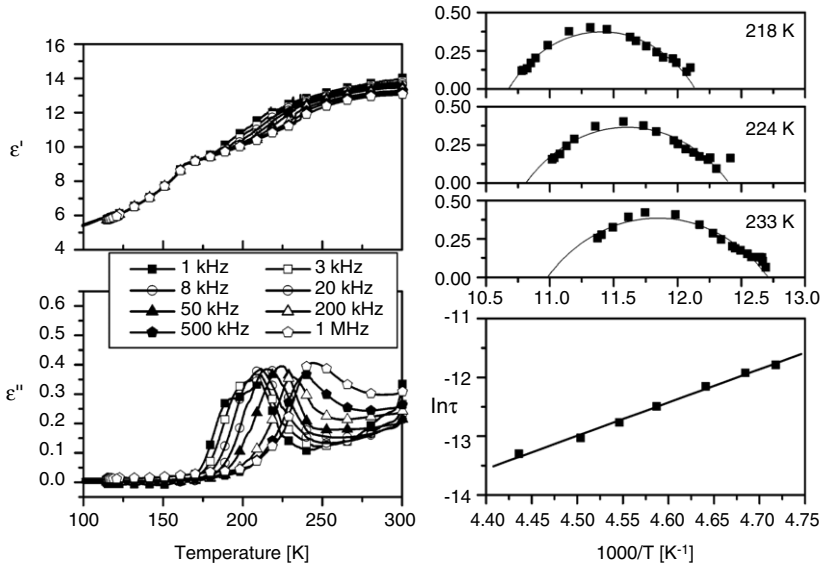

Figure 8. The temperature dependence of the real (left upper part) and the imaginary (left lower part) part of the complex electric permittivity measured along the $[01\bar{1}]$ direction, Cole–Cole diagrams at selected temperatures (right upper part) and $\ln \tau = f(1000/T)$ (right lower part).

one. In this way to estimate the activation energy one can use the Arrhenius relation for the relaxation time:

$$\tau = C \cdot \exp\left(\frac{E_a}{kT}\right) \tag{2}$$

where C is a constant. This activation energy, E_a, represents the potential barrier height of the dipolar reorientation. It was found to be 47 kJ mol^{-1}. This is typical for the relaxation process in molecular–ionic crystals containing large organic cations [15, 16].

3.5. Magnetic resonance studies

3.5.1. ^1H *NMR.* In figure 9 the temperature dependence of the ^{1}H NMR spin–lattice relaxation time, T_1, for [2-CNPyH][ClO_4] is shown. No minimum of the $T_1(1000/T)$ curve is visible. In the whole studied temperature range (100–400 K) the spin–lattice relaxation time decreases from about 4400 s at 91.5 K to about 520 s at 379 K. The decrease of relaxation time is relatively small in this temperature range. On approaching the melting point it begins to shorten, showing critical phenomena behaviour. It should be noted that no visible influence of the phase transition at 170 K on the temperature behaviour of T_1 is observed.

3.5.2. ^{35}Cl *NMR.* An experiment was carried out to find out the role of molecular dynamics of the perchlorate anions in the mechanism of the structural phase transition. Figure 10 shows the ^{35}Cl NMR spectra at two selected temperatures: above (190 K) and below (150 K) the phase transition temperature (170 K) detected by the DSC and dilatometric techniques. One can observe a drastic decrease of the number of lines in the spectra through the phase transition. The 190 K spectrum is more simplified as compared to the 150 K spectrum. These findings allow us to conclude that the ferroelastic transition at 170 K is governed by the dynamics of the perchlorate anions. The freezing out the motion of the $[ClO_4]^-$ moieties below 170 K

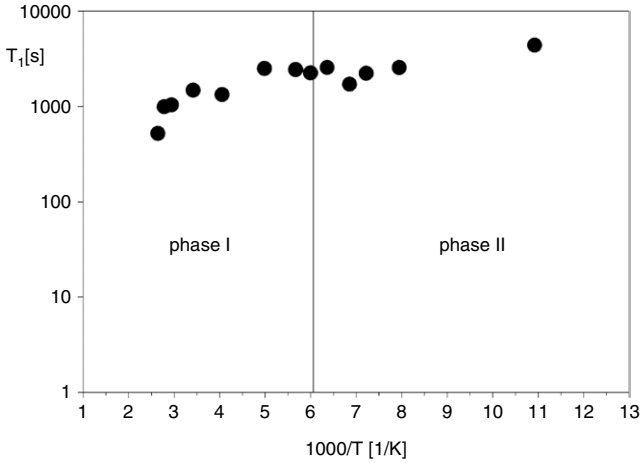

Figure 9. Reciprocal temperature dependence of the ^{1}H NMR spin–lattice relaxation time, T_1, of [2-CNPyH][ClO_4] crystals.

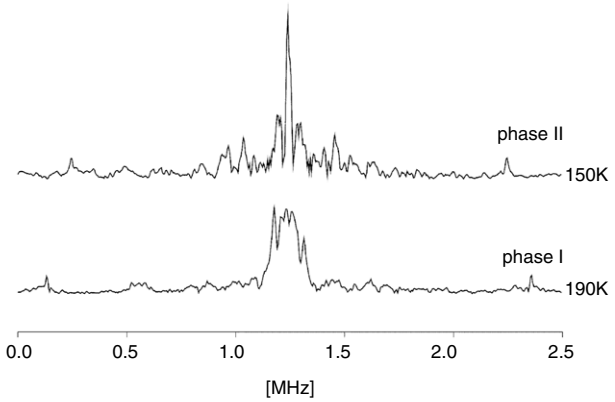

Figure 10. ^{35}Cl NMR spectra at 190 and 150 K.

contributes mainly to the phase transition mechanism. It should be added, on the basis of the ^{1}H NMR measurements, that the dynamics of the 2-cyanopyridinium cations (the overall rotations) plays the minor role in the phase transition mechanism at 170 K.

3.6. IR studies

The FT-MIR (4000–400) cm^{-1} and FT-NIR (500–50) cm^{-1} powder spectra of [2-CNPyH][ClO_4] and 2-cyanopyridine in Nujol at room temperature are shown in figure 11. The assignments and relative intensities of internal vibrations of both moieties are presented in table 4. The assignments of [17–19] were used as guides. The spectra obtained at room temperature show that the structure of the investigated salt is clearly defined. The region of 4000–2000 cm^{-1} is characteristic for stretching vibrations of CH group. It shows two sharp bands at 3120 and 3068 cm^{-1}. The band located at 3268 cm^{-1} with weak intensity was classified as an overtone of two modes: 1631 and 1614 cm^{-1}. The wide weak band at 2348 cm^{-1} is connected with an oscillation of the N–H^{+} bond. It should be noted that the

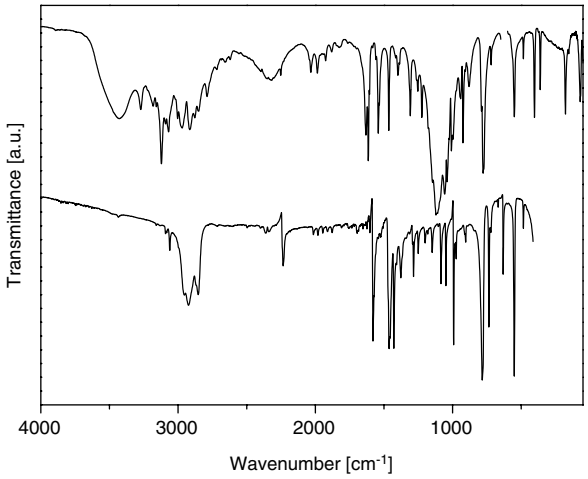

Figure 11. Spectra of [2-CNPyH][ClO_4] crystal in Nujol (upper part) and 2-cyanopyridine in Nujol (lower part) at room temperature.

intensity of the stretching vibration mode of the nitryle group in the 2-cyanopyridinium cation is weak. This band is only just visible on the broad absorption from the N–H^+ band. The benzene finger modes are observed between 2050 and 1780 cm^{-1} as a series of bands with different, rather small intensities. The region 1700–400 cm^{-1} is characteristic of deformation modes of the pyridinium cation and stretching vibrations modes in the $[ClO_4]^-$ anion. When we compare a similar region e.g. 1600–1400 cm^{-1} in the 2-cyanopyridine molecule with the 2-cyanopyridinium cation essential differences are detected. In this region in pyridinium molecule one can notice the following bands: 1635(m), 1581(s), 1533(m), 1521(vs) and 1463(vs). These bands are due to the CN (ring) stretching, C–C stretching and CH bending vibrations. In the 2-cyanopyridinium cation the following sequence is detected: 1631(m), 1614(vs), 1541(m) and 1465(vs) cm^{-1}. As marked in table 4, these differences concern the δCH deformation and νCN stretching modes in the cation. One can expect that the formation of a new (NH^+) band significantly influences the charge distribution in the 2-cyanopyridine ring; in consequence, the bond order changes as well. It also explains the very small intensity of the band assigned to the nitrile group in the investigated compound. The lower-frequency part of spectrum (1200–900) cm^{-1} is characteristic of the internal vibrations of the $[ClO_4]^-$ anion. The group theory gives nine normal modes for isolated $[ClO_4]^-$ moiety with T_d symmetry. In the title compound there were detected three asymmetric stretching vibration modes (1121, 1058 and 1041 cm^{-1}) and one symmetric stretching mode at 925 cm^{-1}. The next three asymmetric deformation modes are assigned to bands at 626, 620 and 478 cm^{-1}.

Figure 12 presents the temperature evolution of the integral intensity of the NH^+ mode at 2348 cm^{-1}. One can observe a continuous increase of the integral intensity of this band with temperature decreasing; however, in the close vicinity of 170 K a clear discontinuous anomaly is visible.

Although the whole infrared spectrum exhibits changes with the decrease of temperature, two regions, assigned to the Cl–O and C–CN oscillations, are presented. These two wavenumber ranges have been chosen, because the most significant changes are observed there. Generally, the changes in the spectrum are not drastic.

Figure 13(a) presents the temperature evolution of bands, and 13(b) the peak positions versus temperature. It is clearly visible, with decreasing temperature, that the band at 534 cm^{-1}

Table 4. Wavenumbers (cm^{-1}) and relative intensities of the bands observed in the infrared spectra of [2-CNPyH][ClO_4] at 290 K (phase I) and 90 K (phase II).

Phase I		Vibrational assignment	Phase II	
3271	vw	Overtone (1631 +1614)	3280	vw
3120	m	CH stretch.	3127	m
3068	w	CH stretch.	3068	w
2348	w broad	CN stretch. + NH^+ stretch.	2325	m broad
2033	sh	Benzene finger	2038	sh
1986	sh	Benzene finger	1992	sh
1925	sh	Benzene finger	1930	sh
1881	sh	Benzene finger	1887	sh
1635	m	C–C stretch.	1640	m
1581	s	CN stretch.	1582	s
1533	m	C–C stretch. + CH bend.	1534	m
1521	m	C–C stretch. + CH bend.	1523	m
1463	vs	Ring stretch.	1465	vs
1399	w	Ring stretch.	1403	w
1377	m	CH bend.	1376	m
1308	m	CH in plane def.	1309	m
1224	m	CH in plane def.	1224	m
1147	s	CH in plane def.	1150	s
1121	vs	ν_{3c} (F) ClO_4 asym. stretch.	1126	vs
1058	vs	ν_{3b} (F) ClO_4 asym. stretch.	1058	vs
1041	s	ν_{3a} (F) ClO_4 asym. stretch.	1042	s
997	s	CH bend.	997	s
941	w	CH out of plane bend.	948	w
925	s	ν_1 (A_1) ClO_4 sym. stretch.	925	s
881	w	CH out of plane	884	w
778	s	Sym. ring breath	774	s
720	w	In plane ring def.	721	w
637	m		640	m
			637	m
632	m		632	m
629	s		629	s
626	vs	ν_4 (F_2) ClO_4 asym. def.	627	vs
			625	s
620	vs	ν_4 (F_2) ClO_4 asym. def.	620	vs
540	s	CCN bend. + in plane ring def.	542	s
			534	s
478	m	ν_4 (F_2) ClO_4 asym. def.	479	m
363	m	CCN out of plane + ring tors.		
178	s	Lattice		
130	m	Lattice		
91	w broad	Lattice		

splits just above the phase transition temperature. The band at 540 cm^{-1} hardens over both phases, but this behaviour in phase II is not as significant as in phase I.

The wavenumber range from 590 to 650 cm^{-1}, assigned to the $[ClO_4]^-$ anions vibrations is presented in figure 14. The biggest changes in the dynamical state of $[ClO_4]^-$ moieties are manifested in the close vicinity of the phase transition temperature. The bands at 637 and at 626 cm^{-1} split approaching 180 K on cooling. The other bands—at 632 and 629 cm^{-1}—harden continuously, whereas the bands at 620 and 616 cm^{-1} soften with decreasing temperature. In order to summarize our spectral investigations we can conclude the following.

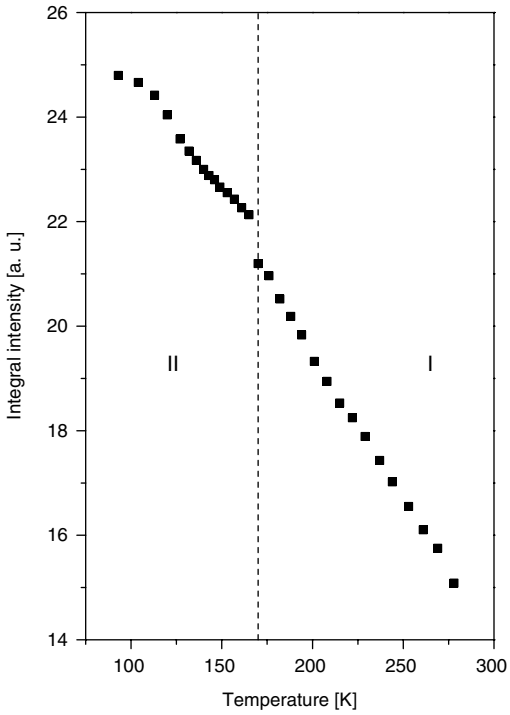

Figure 12. Temperature dependence of the integral intensity of the band at 2348 cm^{-1} of the [2-CNPyH][ClO_4] crystal.

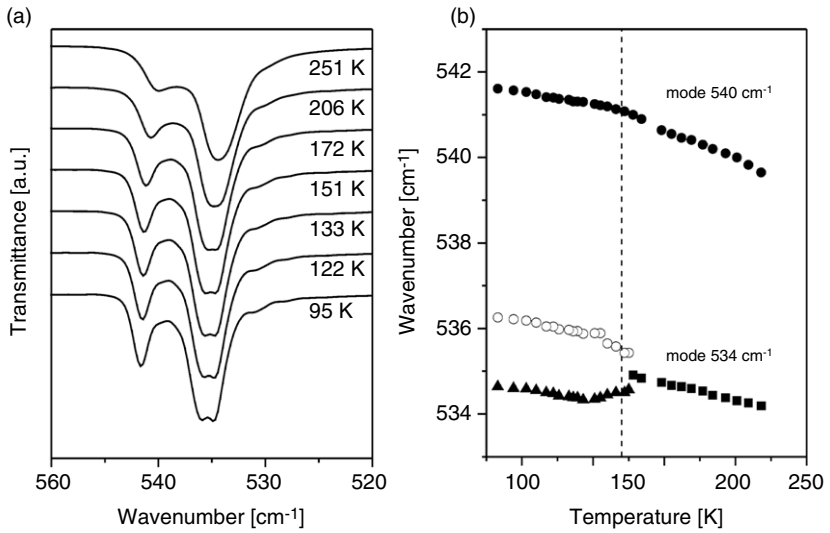

Figure 13. (a) Temperature evolution of the FT-IR spectra in the frequency region assigned to the CCN bands and (b) temperature dependence of the wavenumbers of the symmetric CCN modes of the [2-CNPyH][ClO_4] crystal.

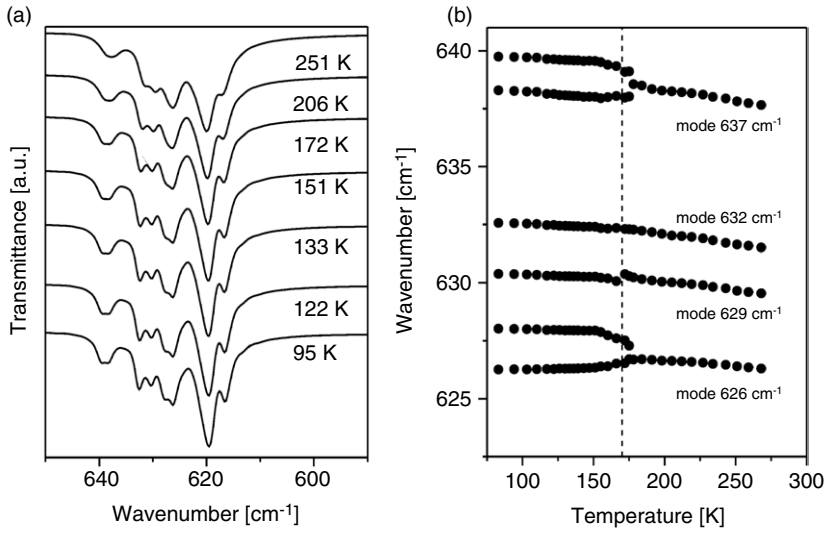

Figure 14. (a) Temperature evolution of the FT-IR spectra in the frequency region assigned to the $[ClO_4]^-$ bands and (b) temperature dependence of the wavenumbers of the $[ClO_4]^-$ modes of the [2-CNPyH][ClO_4] crystal.

(i) Both the cationic and anionic moieties take part in the phase transition. Their contribution to the phase transition mechanism is unexpectedly weak.
(ii) The vibrations that are most sensitive to the phase transition appear to be the C≡N vibrations of the nitryle group, the C–C vibrations of the 2-cyanopyridinium ring and the bending band of the $[ClO_4]^-$ moieties.
(iii) The changes in the distribution of the charge in the 2-cyanopyridinium ring are believed to take place through the phase transition at 170 K.

3.7. Discussion

The comparison of the phase transition sequence and dynamic properties of the title crystal with those found in closely related analogues containing substituted heteroatomic cations, [4-$NH_2C_5H_5N$][ClO_4] [5] and [4-$NH_2C_5H_5N$][BF_4] [6], leads to interesting conclusions. The low-temperature phase transitions in the 4-aminopyridinium salts, resembling that found at 170 K in [2-CNPyH][ClO_4], take place at significantly higher temperatures, 243 and 250 K, in perchlorate and tetrafluoroborate, respectively. The mechanism of the phase transition in 4-aminopyridinium salts was found to be clearly of the order–disorder type and was attributed mainly to the dynamics of the organic cations. Unexpectedly, the low-temperature transition in the 2-cyanopyridinium derivative at 170 K does not exhibit the feature of a pure order–disorder transition. This situation resembles that encountered in numerous alkali perchlorates $MClO_4$ (M = Na, K, Rb, Cs) [20], in which the phase transitions were characterized by both order–disorder and 'displacive' contributions. The first kind of contribution is obviously connected with the motion of the $[ClO_4]^-$ moieties, and the second one with the displacement of the metal atoms. In the title crystal the 2-cyanopyridinium cation may play the same role as the alkali cations in perchlorates. The questions arise, what is the real mechanism of the phase transition in the title crystal, and what is the expected dynamics of the perchlorate anions in the vicinity of the phase transition temperature (170 K)?

The calorimetric and dilatometric studies show that [2-CNPyH][ClO_4] undergoes a clearly continuous phase transition and the crystal experiences subtle structural distortion at 170 K.

The shape of the heat anomaly on the DSC curve suggests the 'displacive' nature of the phase transition. Such a mechanism of phase transition is quite difficult to explain taking into account the presence in the structure dipolar organic cations and possible dynamics of the $[ClO_4]^-$ moieties. The x-ray studies at room temperature clearly show that the 2-cyanopyridinium cation, as a whole, is rigid in the crystal lattice, whereas the polar cyano group is able to perform free rotation about its C–C bond. Nevertheless, at 100 K and probably over the low-temperature phase the –C≡N group is frozen.

The dielectric measurements revealed over the orthorhombic phase (I), before reaching the transition temperature, the relaxation process characterized by a quite small dielectric increment ($\Delta\epsilon_r < 1$). This low-frequency relaxation process may be attributed to the dynamics of the free cyano group, which is bestowed with important dipole moment. On the other hand the dielectric response around the structural phase transition is accompanied by a significant dielectric increment ($\Delta\epsilon_{tr} \approx 20$). The corresponding high-frequency dielectric relaxator seems to be assigned to the dynamics of slightly distorted $[ClO_4]^-$ groups bestowing a permanent dipole moment. These dipolar anionic moieties are able to perform rapid reorientation about their centre of gravity. This is in agreement with the dielectric measurements, since no relaxation process is found over the high-temperature phase in the frequency region up to 30 MHz. Moreover, the biggest dielectric increment is observed in the *c*-direction, i.e., in the direction parallel to the polymer-like structure of cationic and anionic moieties bonded via hydrogen bonds. The changes in the hydrogen bond configuration through the phase transition involve the shift of the centre of gravity of the organic cations with respect to the perchlorate anions. From the crystallographic point of view it leads to an appearance of the 'displacive' contribution in the phase transition mechanism.

The lack of the cationic contributions to the dynamical properties of the title crystal below room temperature is evidenced by the ^1H NMR studies. The T_1 relaxation measurements of the proton magnetic resonance exclude the motion of the cations about its pseudohexagonal C_6 axis in the temperature region below room temperature, and, which is more important, its direct contribution to the phase transition mechanism. On the other hand the ^{35}Cl NMR studies revealed an important change in the dynamical state of the $[ClO_4]^-$ moieties through the 170 K phase transition, which is consistent with the dielectric measurements suggesting the $[ClO_4]^-$ anion contribution to the $\Delta\epsilon_{tr}$ increment. It is worth noting that the $[ClO_4]^-$ moieties are placed in general positions. This means that the change in the dynamical state of the anions does not lead directly to the change of symmetry of the crystal and consequently to the phase transition. The proposed mechanism of phase transition seems to be atypical for this type of crystal. It may be concluded from the experimental results that the mechanism of phase transition is complex. The order–disorder contribution due to the dynamics of the $[ClO_4]^-$ anions (^{35}Cl NMR and dielectric response, $\Delta\epsilon_{tr}$) is evident; however, it plays a minor role in the phase transition mechanism. Thus, the 'displacive' contribution seems to be dominant in the mechanism of phase transition at 170 K.

The pyroelectric studies on [2-CNPyH][ClO_4] clearly showed that this crystal possessed the polar properties over the phase II; however, the spontaneous polarization was not found to be reversible. This means that the dipole–dipole interactions are too weak to lead to ferroelectric order. The x-ray measurements made at different temperatures show that the phase transition in [2-CNPyH][ClO_4] is of ferroic (ferroelastic) type, because it is accompanied by a change in the symmetry of crystal. We made an effort to observe the ferroelastic domain structure under a polarizing microscope. Unfortunately we did not observe it, most probably, because the domains were too fine. According to Sapriel's approach the phase transition at 170 K belongs to the ferroelastic species 222F2 [21].

We should stress that [2-CNPyH][ClO_4] is a potential nonlinear material and a polar one, over phase I (space group $P2_12_12_1$) and over phase II ($P2_1$), respectively. The role of the hydrogen bonds, such as O–H $\cdots$ O, N–H $\cdots$ O and C–H $\cdots$ O, in numerous nonlinear optical (NLO) crystals has been extensively studied in the last decade. Xue *et al* [22–25] have recently reported the influence of the hydrogen bonds on the optical nonlinearities of inorganic crystals, such as HIO_3, $(NH_4)H_2PO_4$ and $K_2La(NO_3)_5{\cdot}2H_2O$. It has been clearly shown that hydrogen bonds play a very important role in NLO contributions to the total nonlinear properties. In the case of the [2-CNPyH][ClO_4] crystal the change in the C–H $\cdots$ O hydrogen bond geometry (geometrical flexibility), through the phase transition, seems to be one of the most important contributions to the total crystal nonlinearity.

3.8. Conclusions

(i) The structure of [2-CNPyH][ClO_4] is built of discrete anions and cations, which are connected to each other via N–H $\cdots$ O hydrogen bonds of intermediate strength.
(ii) The title compound undergoes a continuous, ferroic (ferroelastic) phase transition at 170 K of the 222F2 type.
(iii) The mechanism of the phase transition is complex. Both 'order–disorder' and 'displacive' contributions are postulated to exist.
(iv) The crystal reveals pyroelectric properties below 170 K.
(v) The x-ray and pyroelectric measurements indicate that the [2-CNPyH][ClO_4] crystal is a potential nonlinear optical material. The change in the C–H $\cdots$ O hydrogen bond configuration contributes to the total nonlinear properties of this crystal.

References

[1] Pająk Z, Czarnecki P, Wąsicki J and Nawrocik W 1998 *J. Chem. Phys.* **109** 6420
[2] Pająk Z, Czarnecki P, Małuszyńska H and Szafrańska B 2000 *J. Chem. Phys.* **113** 848
[3] Pająk Z, Małuszyńska H, Szafrańska B and Czarnecki P 2000 *J. Chem. Phys.* **117** 5303
[4] Pająk Z, Czarnecki P, Szafrańska B, Małuszyńska H and Fojud Z 2004 *Phys. Rev.* B **69** 132102
[5] Czupiński O, Bator G, Ciunik Z, Jakubas R, Medycki W and Świergiel J 2002 *J. Phys.: Condens. Matter* **14** 8497
[6] Czupiński O, Jakubas R and Pietraszko A 2004 *J. Mol. Struct.* **704** 177
[7] Sheldrick G M 1997 *SHELXS-97. Program for the Solution of Crystal Structure* University of Göttingen, Germany
[8] Sheldrick G M 1997 *SHELXL-97. Program for the Refinement of Crystal Structure* University of Göttingen, Germany
[9] Sheldrick G M 1990 *SHELXTL. Siemens Analytical X-ray Instruments Inc.* Madison, Wisconsin, USA
[10] Ohkoshi S, Arimoto Y, Hozumi T, Seino H, Mizobec Y and Hashimoto K 2003 *Chem. Commun.* 2772
[11] Blake A J, Champness N R, Nicolson J E B and Wilson C 2001 *Acta Crystallogr.* C **57** 1290
[12] Ni J, Li Y-Z, Xue Z, Chen H-L and Wang Z-L 2003 *Acta Crystallogr.* C **59** m201
[13] Barnes J C and Weakley T J R 1978 *Acta Crystallogr.* B **34** 1984
[14] Fedeli W and Mazza F 1976 *Acta Crystallogr.* B **32** 878
[15] Bednarska-Bolek B, Ciunik Z, Jakubas R, Bator G and Ciąpala P 2002 *J. Phys. Chem. Solids* **63** 507
[16] Tarasiewicz J, Jakubas R, Baran J and Pietraszko A 2004 *J. Mol. Struct.* **697** 161
[17] Evans J C 1960 *Spectrochim. Acta* **16** 428
[18] Pejov L and Petruševski V M 2002 *J. Phys. Chem. Solids* **63** 1873
[19] Wong P T T 1983 *J. Chem. Phys.* **78** 4840
[20] Lin J, Duan C, Mei W N, Smith R W and Hardy J R 2002 *J. Solid State Chem.* **163** 294
[21] Sapriel J 1975 *Phys. Rev.* B **12** 5128
[22] Xue D and Zhang S 1999 *Chem. Phys. Lett.* **301** 449
[23] Xue D and Ratajczak H 2003 *Chem. Phys. Lett.* **371** 601
[24] Xue D and Ratajczak H 2005 *J. Mol. Struct.: THEOCHEM* **716** 207
[25] Xu D, Xue D and Ratajczak H 2005 *J. Mol. Struct.* **740** 37